Multiscale study on the shearing behaviour of unsaturated basalt fibre modified red mudstone as subgrade fill material

Jiahang Xu[1,2], *Dariusz* Wanatowski[4,*], *Xianfeng* Liu [2,3], *Shengyang* Yuan [2,3], and *Jie* Ma[2,3]

[1] SWJTU-Leeds Joint School, 111 Second Ring Road of North Section 1, China.

[2]Southwest Jiaotong University, Key Laboratory of High-Speed Railway Engineering, Ministry of Education, 111 Second Ring Road of North Section 1, China.

[3]Southwest Jiaotong University, School of Civil Engineering, 111 Second Ring Road of North Section 1, China.

[4] University of Leeds, Faculty of Engineering and Physical Sciences, Woodhouse Lane, Leeds LS2 9JT, United Kingdom.

Abstract. High-speed railway development in Southwest China often involves traversing vast areas of red mudstone, a material with poor mechanical properties unsuitable for subgrade applications. This study proposes the use of basalt fibre to enhance the shearing performance of the unsaturated red mudstone fill material over a broad range of degree of saturation. A series of direct shear tests were conducted to analyse the influence of degree of saturation and basalt fibre content, accompanied by scanning electron microscopy to investigate the underlying microscale mechanisms. The results show that the cohesion of untreated red mudstone initially increases but subsequently decreases with rising degree of saturation, while the internal friction angle consistently diminishes. An increased degree of saturation also leads to a reduced brittleness and a lower dilatancy angle. The observed shearing behaviours are classified into three distinct types: softening-dilation, hardening-dilation, and hardening-contraction. The maximum cohesion occurs at the optimal degree of saturation and fibre content, although the internal friction angle decreases as fibre content and degree of saturation increase. Furthermore, the brittleness index reduces considerably with a higher fibre content, and the hardening-dilation stage occurs earlier compared to untreated red mudstone. The improvements are attributed to the formation of 3D-grid structures within the basalt fibre modified red mudstone, enhancing particle connectivity. This study provides essential insights into addressing subgrade stability challenges in red bed regions through basalt fibre modification, while also presenting a sustainable approach to repurposing red mudstone construction waste in engineering applications.

1 Introduction

In Southwest China, the expansive development of high-speed railways necessitates traversing regions rich in red mudstone, a geological material noted for its deleterious properties which significantly challenge construction endeavours [1–3]. Characteristically, red mudstone is prone to disintegration and softening upon moisture exposure, a situation further exacerbated by the region's hot and humid climate [4–6]. Such climatic conditions induce substantial variations in the degree of saturation of red mudstone, markedly influencing its mechanical properties and, by extension, impacting railway operational integrity.

Confronted with these challenges, there is an imperative need for the development of robust engineering solutions to enhance the structural qualities of red mudstone. Recent research has underscored the potential of fibres as sustainable materials that can significantly enhance the strength and ductility of soil. These studies have consistently shown that the integration of various fibres, including plant, polypropylene [7], polyester, and basalt fibres [8–14], can substantially improve both the shear strength and elastic modulus of soils. Amongst these fibres, the utilisation of basalt fibre emerges as a particularly promising method in this context. Known for its superior tensile strength, low water sensitivity and strong acid-alkali resistance, basalt fibre offers a means to significantly improve the shear strength of red mudstone [15–18]. This unique combination of properties makes basalt fibre an optimal choice for soil modification, especially in environments that pose significant geotechnical challenges.

Despite the extensive development of high-speed railway infrastructure across Southwest China, the region's geological landscape is dominated by red mudstone, which presents significant engineering challenges due to its unfavourable properties. While previous studies have explored various stabilisation techniques, the potential of basalt fibre to address the shearing behaviour of red mudstone under wide degree

* Corresponding author: D.Wan@leeds.ac.uk

of saturation has not been fully investigated. Moreover, the mechanisms underlying the modification of red mudstone through the addition of basalt fibre and its impact on shearing behaviour remain inadequately understood. This study aims to fill this gap.

In this research, direct shear tests were performed on the untreated red mudstone fill material and the basalt fibre modified filler, examining various conditions including different degrees of saturation and fibre contents. These conditions were then further investigated by scanning electron microscopy (SEM). The findings were analysed using the Mohr-Coulomb failure criterion, exploring the relationship between strength and dilation under different initial conditions of the specimens. Additionally, the reinforcement mechanics was studied, focusing on the interaction between the soil particles and basalt fibres. This study explores the addition of basalt fibre to enhance the mechanical properties of red mudstone for railway subgrade, offering a sustainable solution to improve structural stability and repurpose red mudstone construction waste.

2 Materials and experimental programme

2.1 Materials

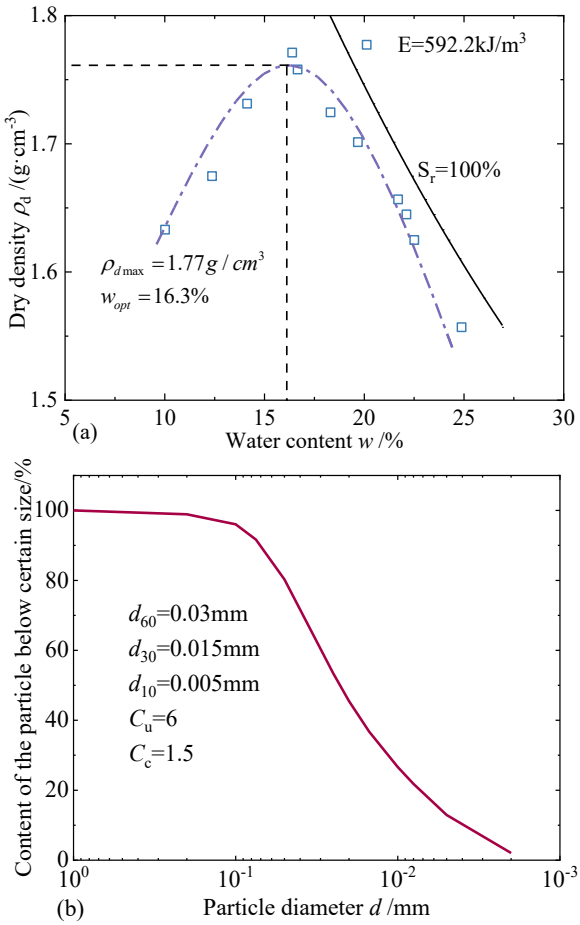

Fig. 1. (a) Compaction curve, (b) Grading curve.

The basic physical properties of the red mudstone used in the research are shown in Table 1. According to the results of the Proctor compaction test, the maximum dry density was 1.77 g/cm³, and the optimum degree of saturation was 16.3%, as illustrated in Fig. 1. Besides, the coefficient of uniformity Cu=6 and the coefficient of curvature Cc=1.5. In terms of the basalt fibre, the length and diameter were 16μm and 10mm, respectively. The elastic modulus and tensile strength were 81GPa and 4300MPa. Further information about the materials can be found in [19].

Table 1. Basic physical properties.

Liquid limit /%	Plastic limit /%	Specific gravity	Particle size /mm
32.5	13.8	2.69	⩽1

2.2 Experimental programme and methods

This study focused on characterising the shearing behaviour of basalt fibre modified red mudstone (BFRM), particularly examining the influence of initial degree of saturation and fibre content. Degrees of saturation were adjusted over a broad spectrum to encompass two extremes: from a very dry state (23.1% saturation) to a fully saturated state (99.8%). To adhere to subgrade construction standards [20], the degree of compaction was 0.95, which means the dry density was 1.7g/cm³. It should be noted that previous research [21,22] has identified that the maximum cohesion in similar materials typically occurs at a degree of saturation of approximately 60%. Consequently, the experiments on fibre content were conducted under this specific degree of saturation to ensure relevance and accuracy. Moreover, all the specimens were statically compacted with 61.8mm in diameter and 20mm in height.

The direct shear tests were performed using an apparatus manufactured by Geocomp with the shearing rate of 1 mm/min and the maximum shearing displacement of 10 mm. Six different vertical stresses were applied to reflect the depth of the subgrade. Table 2 shows the overall information of the direct shear testing.

To elucidate the improvement mechanism of BFRM, scanning electron microscopy (SEM) tests were employed to investigate the microscale features of specimens, both with and without fibre, under various conditions, as detailed in Table 3. The SEM examination was conducted using a JSM-IT500 apparatus.

Table 2. Direct shear test programme.

Dry density /g· cm³	Degree of saturation /%	Fibre content /%	Vertical stress /kPa
1.7	23	0	25, 50, 100, 200, 300, 400
	40	0	
	60	0, 0.1, 0.2, 0.3, 0.4	
	74	0	
	Sat	0	

Table 3. Microstructure test programme.

Dry density /g· cm^3	Degree of saturation /%	Fibre content /%	Curing age /day
1.7	60	0	----
	Sat	0	----
	Sat	0.2	28

3 Results and discussion

3.1 Shearing behaviour of the untreated red mudstone fill material

Fig. 2(a) illustrates the evolution of stress-displacement curve with the change of degree of saturation and Fig. 2(b) presents the peak and residual stress. It can be observed that the peak strength tends to increase with the increase of the degree of saturation and then decrease with a peak value of S_r=60%. Besides, it gradually varies from softening to hardening mode.

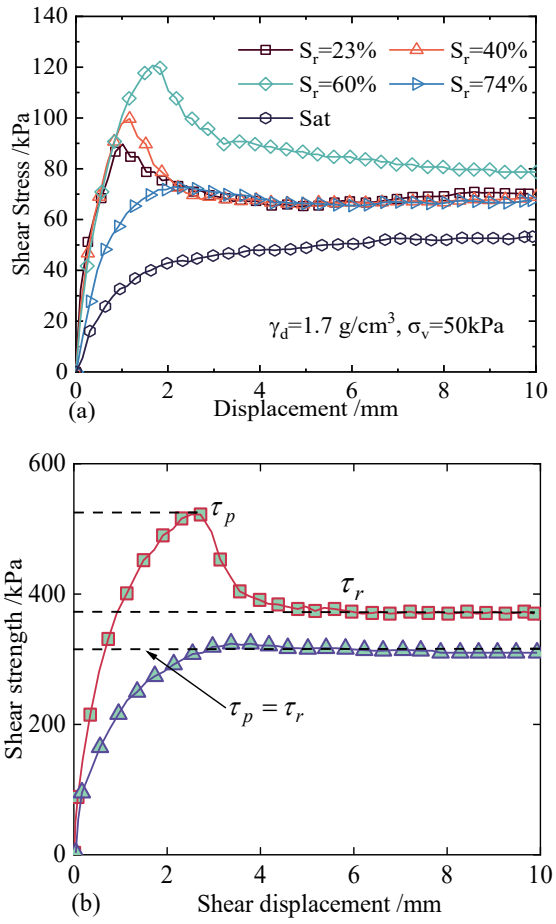

Fig. 2. (a) Effect of degree of saturation on the stress-displacement curve at ρ_d=1.7g/cm^3, σ_v=50kPa, (b) Schematic demonstration of peak stress and residual stress.

Fig. 3 presents the variation of peak strength, cohesion, and internal friction angle with degree of saturation. Notably, the internal friction angle exhibits a steady decrease as saturation increases. This trend is attributed to the formation of a water film around soil particles as saturation rises, which serves to reduce the friction between them. Additionally, this process leads to a reduction in the interlocking among the soil particles. Regarding the cohesion, the peak value is observed at S_r=60%, closely aligning with the phenomenon of stress-displacement curve. When the degree of saturation is below this optimum level, the particles are in direct contact, resulting in dominant friction and a robust bonding effect. As the degree of saturation increases, water films form, acting to reduce the friction between the soil particles.

As shown in Fig. 4, the brittleness index (I_b) for unsaturated specimens, defined as the ratio of peak shear strength to residual shear strength, exhibits a decreasing trend with increasing degree of saturation. The increase of degree of saturation leads to smaller differences between the peak and residual shear strengths, resulting in a lower brittleness index. In contrast, for specimens in the saturated state, the stress-displacement curves present a hardening mode, the brittleness index remains equal to 1.

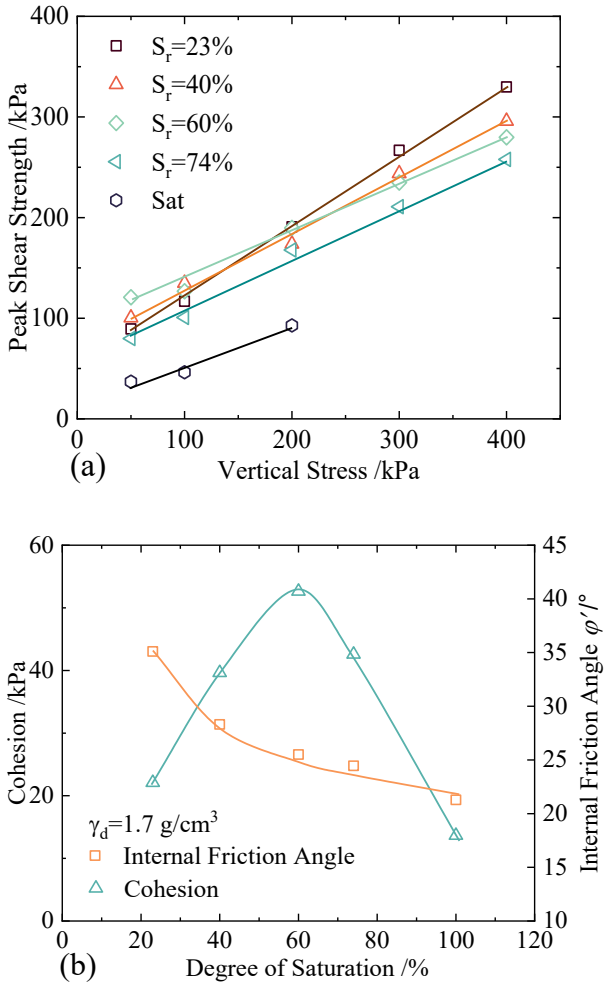

Fig. 3. (a) Effect of degree of saturation on peak shear strength. (b) Effect of degree of saturation on cohesion and internal friction angle.

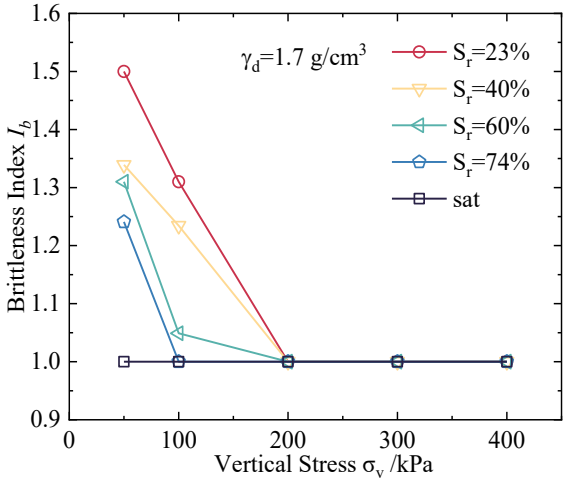

Fig. 4. Effect of degree of saturation on brittleness index.

Fig. 5(a) illustrates the typical relationship between the shear and vertical displacement for specimens with a degree of saturation of approximately 60%. Herein, positive displacement indicates compression, while negative displacement signifies swelling. As the vertical stress increases, the specimen's behaviour transitions from dilation to contraction, and a specific vertical stress defines the boundary between these two states. This volumetric change in the specimens is closely linked to their shearing behaviour, commonly assessed through specimen dilatancy, as highlighted by Reynolds [23]. Bolton [24] defines the dilatancy angle as the ratio of the increment of vertical displacement to the one of shear displacement, as shown in Fig. 5(b) and expressed by the following formula:

$$\psi = -arctan\frac{\Delta y}{\Delta x} \quad (1)$$

Fig. 5(c) illustrates the evolution between the vertical stress and dilatancy angle at varying degrees of saturation. For a given degree of saturation, the dilatancy angle consistently reduces as vertical stress increases. This trend can be attributed to the denser internal arrangement of the particles under the higher vertical stress conditions. At a constant vertical stress, the dilatancy angle diminishes with increasing degree of saturation, while under saturated state, the dilatancy angle may even become negative, likely due to the collapse of the pores within the specimen.

3.2 Shearing behaviour of the basalt fibre modified red mudstone fill material

Fig. 6 illustrates the evolution of the stress-displacement curve with the change of fibre content. To make the evolution process clearer, only 0, 0.2 and 0.4% are presented. The peak shear strength would initially increase and then decrease while the fibre content exceeds c_{bf}=0.2%, indicating that this is the optimal fibre content. The previous research [25] showed that the fibre forms a three-dimensional network that increases the friction between the fibre and the soil. Yet, an overabundance of fibre results in irregular distribution and prevents separation into fine strands. This diminishes the interaction surface between the soil particles and the fibres, causing a reduction in friction and strength. The evolution of basalt fibre content on the peak shear strength could align with it (see Fig.7). Fig. 7(b) illustrates the effect of fibre content on the peak cohesion and internal friction angle. As identified previously, 0.2% is the optimal fibre content. When c_{bf}<0.2%, the peak cohesion increases, but beyond this threshold (c_{bf}>0.2%), it declines. Conversely, the internal friction angle decreases consistently with increasing fibre content.

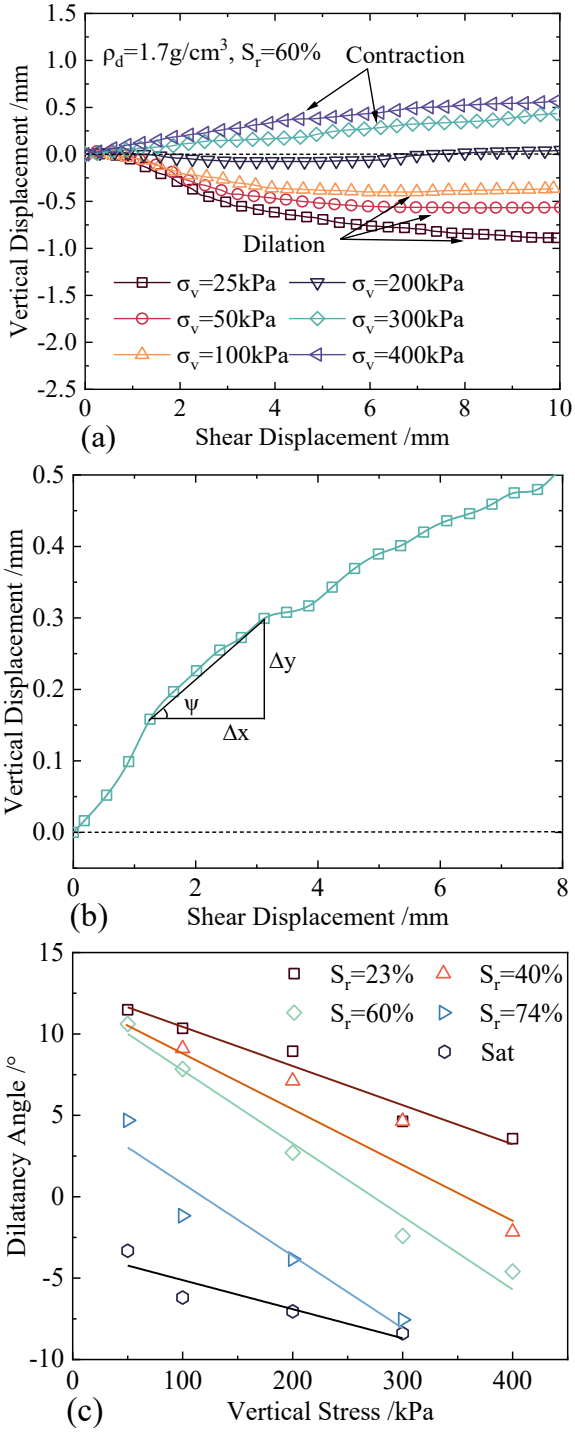

Fig. 5. (a) Influence of vertical stress on vertical displacement. (b) Schematic demonstration of dilatancy angle calculation. (c) Effect of degree of saturation on dilatancy angle.

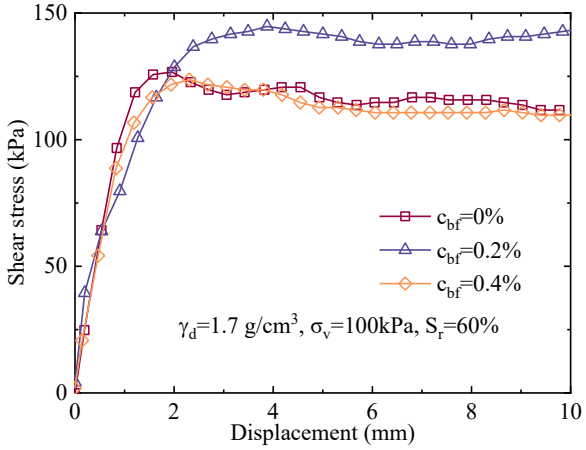

Fig. 6. Influence of fibre content on stress-displacement curve.

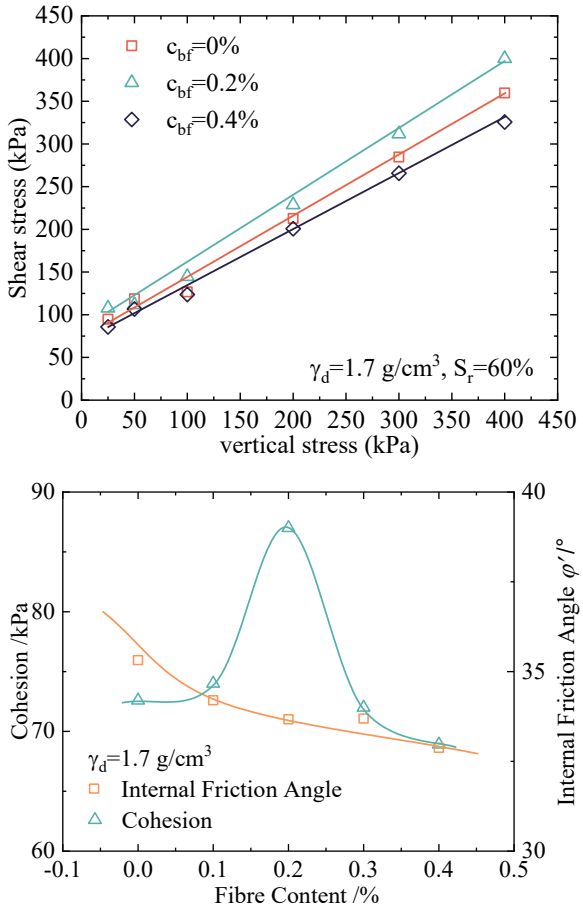

Fig. 7. (a) Influence of fibre content on peak shear strength. (b) Influence of fibre content on cohesion and internal friction angle.

Fig. 8 shows that the shear responses of the specimens transfer from softening to hardening as the vertical stress increases, moving towards a brittleness index of 1. Furthermore, the addition of fibre significantly influences the shear behaviour, markedly reducing brittleness. This indicates that basalt fibre enhances the strength characteristics of the material, shifting the shear response towards a hardening mode.

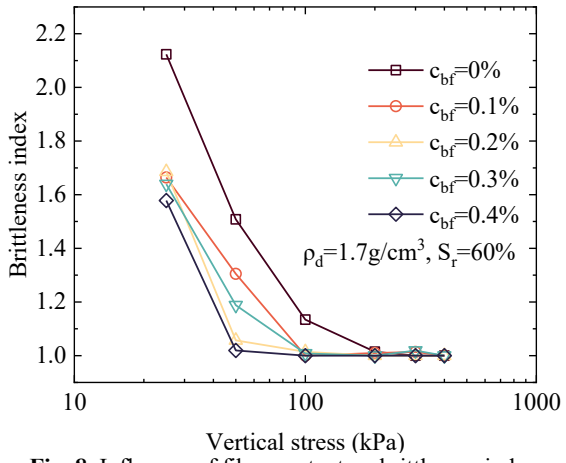

Fig. 8. Influence of fibre content on brittleness index.

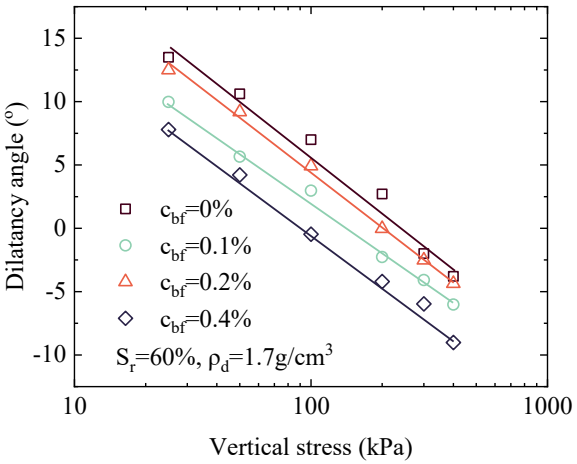

Fig. 9. Influence of fibre content on dilatancy angle.

Fig. 9 shows the influence of fibre content on dilatancy angle. It clearly demonstrates that basalt fibre tends to reduce the magnitude of the dilatancy angle, indicating the significant impact of fibre on modifying material's shearing characteristics.

Fig. 10 reveals the relation between the dilatancy angle and the brittleness index for BFRM and untreated red mudstone. The curve can be segmented into three stages, designated as Stage S1 to S3. In Stage 1 (Softening-Dilation), the brittleness index exceeds 1, and the dilatancy angle is greater than 0°. Additionally, a rapid decrease in the brittleness index occurs as the dilatancy angle diminishes. Moving to Stage 2 (Hardening-Dilation), the brittleness index decreases to 1, while the dilatancy angle remains positive. Unlike Stage 1, the dilatancy angles continue to vary, but the brittleness index remains constant. Finally, in Stage 3 (Hardening-Contraction), the brittleness index stabilizes at 1, akin to Stage 2, but the dilatancy angle drops below 0°. Interestingly, in comparison with untreated red mudstone, at a given brittleness index, the dilatancy angle for BFRM specimens is consistently lower. This suggests an enhancement in the ductility of red mudstone following the addition of basalt fibre. Such improved performance can enhance the behaviour of subgrades constructed from red mudstone, potentially reducing deformation.

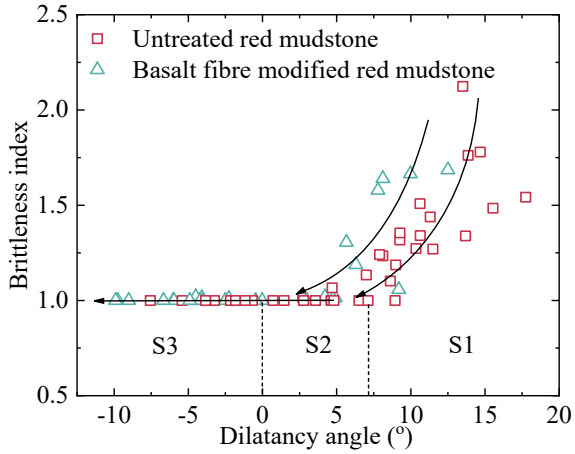

Fig. 10. Change of brittleness index with dilatancy angle.

3.3 The microstructure features of the basalt fibre modified red mudstone fill material

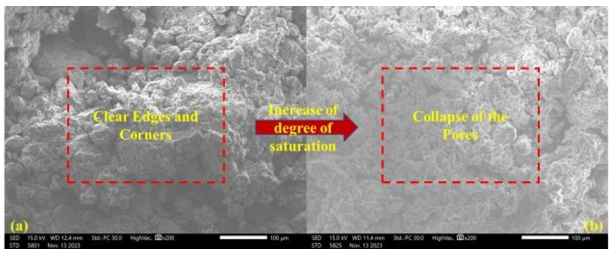

Fig. 11. SEM images of the untreated red mudstone with degree of saturation of (a)S_r=60%; (b) S_r=100%.

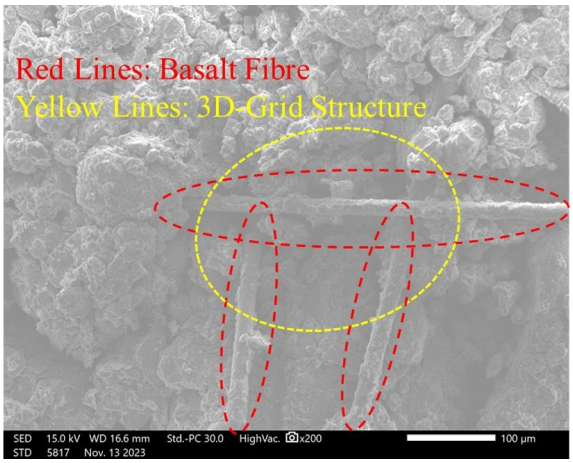

Fig. 12. SEM of the basalt fibre modified red mudstone.

Fig.11 illustrates the morphological changes in untreated red mudstone before and after reaching saturation. Fig. 11(a) displays the mudstone at its optimal degree of saturation, featuring well-defined particle edges and corners with many visible pores. As the mudstone transitions to a saturated condition, shown in Fig. 11(b), the clear spaces between particles diminish and the sharp edges and corners become less distinct. Particles with defined edges typically resist movement more effectively, which is linked to the increased shear strength in unsaturated red mudstone compared to their saturated equivalents, as demonstrated in Fig. 3.

Fig. 12 shows the morphology of BFRM specimens, illustrating how soil particles encapsulate the basalt fibres. The exceptional tensile strength of these fibres strengthens the interlaced soil particles. Additionally, as basalt fibres accumulate, they may overlap or be enveloped by individual soil particles, promoting the formation of 3D-grid structures. These structures potentially improve the connectivity among adjacent soil particles, enhancing the overall structural integrity.

4 Conclusions

This study investigates the effect of basalt fibre to enhance the shearing performance of the unsaturated red mudstone fill material over a broad range of degree of saturation. The results show that incorporating basalt fibre significantly improves the strength and deformation characteristics of the red mudstone, which is essential for minimising subgrade stability hazards in red bed regions of Southwest China. The main conclusions are as follows:

(1) The cohesion of the untreated red mudstone fill material initially rises, then falls as the degree of saturation decreases. The internal friction angle demonstrates a downward trend with decreasing degree of saturation. The shearing behaviour can be categorised into three types: Softening-Dilation, Hardening-Dilation, and Hardening-Contraction.

(2) In terms of the basalt fibre modified red mudstone, the maximum cohesion is achieved at the optimal degree of saturation and fibre content. Nonetheless, increasing either the fibre content or the degree of saturation results in a reduction of the internal friction angle. Moreover, a higher fibre content leads to a marked decrease in the brittleness index, and the Hardening-Dilation mode commences earlier than in the untreated red mudstone.

(3) SEM analysis of the tested material demonstrates that the enhancement can be attributed to the creation of 3D grid structures within the basalt fibre modified red mudstone, which in turn improves particle connectivity.

References

[1].C. Zhang, G. Jiang, X. Liu, and O. Buzzi, Comput. Geotech. **77**, 11 (2016).

[2].C. Zhang, G. Jiang, L. Su, and W. Liu, J. Mt. Sci. **15**, 1789 (2018).

[3].J. Xu, X. Liu, J. Ma, and S. Yuan, *IOP Conf. Ser. Earth Environ. Sci.* **1332**, 012013 (2024).

[4].W. Chen, G. Jiang, H. Zhao, L. Wu, and A. Li, J. Cent. South Univ. **21**, 4690 (2014).

[5].K. Chen, X.-F. Liu, S.-Y. Yuan, S.-X. Pan, J. Ma, and G.-L. Jiang, Soil Dyn. Earthq. Eng. **162**, 107497 (2022).

[6].China Railway First Survey and Design Institute Group Co., Ltd., *Code for design on subgrade of railway* (2005).

[7].M. Chen, S.-L. Shen, A. Arulrajah, H.-N. Wu, D.-W. Hou, and Y.-S. Xu, Geotext. Geomembr. **43**, 515 (2015).

[8].N. Ranjbar and M. Zhang, Cem. Concr. Compos. **107**, 103498 (2020).

[9].N. Ramdani, M. Derradji, and E. O. Mokhnache, Mater. Today Commun. **31**, (2022).

[10].I. Fidan, A. Imeri, A. Gupta, S. Hasanov, A. Nasirov, A. Elliott, F. Alifui-Segbaya, and N. Nanami, Int. J. Adv. Manuf. Technol. **102**, 1801 (2019).

[11].S. Paul, M. S. Islam, and N. Chakma, Constr. Build. Mater. **427**, 136290 (2024).

[12].S. Paul, M. S. Islam, and M. I. Hossain, Constr. Build. Mater. **409**, 134224 (2023).

[13].G. Araya-Letelier, F. C. Antico, C. Burbano-Garcia, J. Concha-Riedel, J. Norambuena-Contreras, J. Concha, and E. I. Saavedra Flores, Constr. Build. Mater. **276**, 122127 (2021).

[14].M. Islam, S. Paul, and M. Hossain, in (2023), pp. 2444–2448.

[15].V. Dhand, G. Mittal, K. Y. Rhee, S.-J. Park, and D. Hui, Compos. Part B Eng. **73**, 166 (2015).

[16].M. Li, D. Xing, Q.-B. Zheng, H. Li, B. Hao, and P.-C. Ma, Constr. Build. Mater. **316**, (2022).

[17].H. Jamshaid and R. Mishra, J. Text. Inst. **107**, 923 (2016).

[18].C. Gao, G. Du, Q. Guo, H. Xia, H. Pan, and J. Cai, J. Mater. Civ. Eng. **32**, 06020014 (2020).

[19].J. Xu, X. Liu, J. Ma, S. Yuan, L. Zhang, and F. Chen, Constr. Build. Mater. **456**, 138961 (2024).

[20].Ministry of Railways of the People's Republic of China, *Code for design of high speed railway* (2015).

[21].Z. Li, F. Chen, J. Ren, and Z. Chen, Coatings **13**, 532 (2023).

[22].J. Chen, J. Mu, A. Chen, Y. Long, Y. Zhang, and J. Zou, Sustainability **16**, 7579 (2024).

[23].O. Reynolds, Lond. Edinb. Dublin Philos. Mag. J. Sci. **20**, 469 (1885).

[24].M. D. Bolton, Géotechnique **36**, 65 (1986).

[25].X. Duan and J. Zhang, Adv. Mater. Sci. Eng. 2019, e9561794 (2019).